An Efficient, General-Purpose Technique to Identify Storm Cells in Geospatial Images

Valliappa Lakshmanan[1,2]*, Kurt Hondl[2], Robert Rabin[2]

*Corresponding author: V Lakshmanan, 120 David L. Boren Blvd, Norman OK 73072; lakshman@ou.edu

[1]Cooperative Institutute of Mesoscale Meteorological Studies, University of Oklahoma; [2]National Oceanic and Atmospheric Administration / National Severe Storms Laboratory

ABSTRACT

Existing techniques to identify, associate and track storms rely on heuristics and are not transferrable between different types of geospatial images. Yet, with the multitude of remote sensing instruments and the number of channels and data types increasing, it is necessary to develop a principled and generally applicable technique. In this paper, an efficient, sequential, morphological technique called the watershed transform is adapted and extended so that it can be used for identifying storms. The parameters available in the technique and the effect of these parameters are also explained.

The method is demonstrated on different types of geospatial radar and satellite images. Pointers are provided on the effective choice of parameters to handle the resolutions, data quality constraints and dynamic range found in observational datasets.

```
@Article{stormattr,
  author =       {Valliappa Lakshmanan and Travis Smith},
  title =        {Data Mining Storm Attributes from Spatial Grids},
  journal =      {J. Ocea. and Atmos. Tech.},
  year =         {2009},
  volume =       {26},
  number =       {11},
  pages =        {2353-2365}
}
```

1. Introduction

Identifying storms from remotely sensed imagery such as radar and satellite fields is a fundamental problem in automated weather analysis and guidance tools. Once storms are identified, they can be used to compute storm properties for classification. Trends in the properties of the identified entities can be presented to a decision maker.

A storm in weather imagery is a region of high intensity separated from other areas of high intensity. The "intensity" depends on the weather data in question: reflectivity from weather radar, flash density from cloud-to-ground lightning observations or infrared temperature from weather satellite may all be used. High intensities may not always correspond to storms. For example, high radar reflectivity could be result of anamolous propagation. Low infrared temperatures may be because the earth's surface is itself cold and not because of high-altitude clouds. In practice, storm identification will have to be preceded by a preprocessing step that corrects for such sensor-specific details. The intensity threshold chosen as indicative of a storm depends on the field being segmented and the type of storms desired. Thus, an application interested in multicell storms would use lower reflectivity thresholds than one interested only in individual convective cells.

Storm identification in remotely sensed images has proven resistant to general approaches. The problems associated with storm identification can been side-stepped in some cases by processing rectangular subgrids of images. For example, Tag et al. (2000) classify clouds by processing 16x16 pixel areas while Rinehart and Garvey (1978) estimate motion by maximizing the correlation between constant-size subgrids of successive images. However, such methods compromise the ultimate classification or motion estimates: incorporation of storm

properties rather than just region properties ought to yield better classification results while maximizing the match between the moving entities rathern than just subgrids ought to yield better motion estimates.

The simple approach to identifying storms is to threshold the image based on a physically reasonable value. For example, Augustine and Howard (1988) describe an automated identification method for mesoscale convective complexes (MCCs). Candidate MCCs were identified by thresholding the satellite infrared image at a temperature of $221K$. Contiguous pixels were combined through a process known in image processing as *region growing* (Jain 1989) and the area, duration and eccentricity of these regions were used to determine whether the region in question was a MCC.

A simple schematic of using a threshold is shown in Figure 1a. For clarity, a one-dimensional intensity function is shown. All the discussions based on the 1D functions extend quite naturally to images: the position in an image would be a pixel and the intensity function would be defined on the x-y plane. Also, for clarity, all diagrams and text assume that cells consist of high intensity regions. In images such as infrared satellite images, where cold cloud tops are of interest, one would look for minima, not maxima, but the principles involved remain the same.

Using a single, hard threshold is subject to one glaring problem. The threshold is global in nature and applies to the entire image. Mature storms may be more intense and cover a large area, but initiating cells may have only a few points above the threshold. Thus, based on a single threshold, it is not possible to distinguish between noisy points (some of which may happen to be above the chosen threshold) and initiating cells which may have only a few points above the threshold. In order to identify initiating cells in a different

location, it may be desirable to lower the threshold, but this has the undesirable side effect of greatly increasing the area of mature cells. This is not a problem when analyzing large-scale systems after the fact, but is a critical short-coming when identifying cells over large areas for guidance purposes.

To avoid the problem of initiating cells having only a few pixels above threshold, a method called *hysteresis* (Jain 1989) can be employed. The term hysteresis comes from the lag observed between the application of an electromagnetic field and its subsequent effect on a material. In the image processing context, the lagging effect is provided by the use of two thresholds – one to start the thresholding and the other (a lagging one) to stop it. Thus, two thresholds are maintained and a cell is defined as contiguous pixels above the second (lower) threshold as long as it contains a certain area above the first (higher) threshold. This is shown in Figure 1b. The hysteresis technique can be further improved by using a threshold that varies throughout the image, rather than a single, global threshold.

Both the above improvements to the basic thresholding technique have been incorporated in storm identification methods on weather radar images. For example, Crane (1979) defined the hysteresis level to be 3dBZ below the threshold being used. Rosenfeld (1987) defined the threshold to be used as the nearest local maximum in the neighborhood of the pixel, provided that it was at least 2 dBZ stronger than every other adjacent maximum. Thresholding techniques involving simple heuristics perform well on individual cases, but require multiple changes in order to work in operational situations where a diverse set of storms may be expected throughout any given year (Rosenfeld 1987).

In the United States, the operational way to identify storms from radar images is that of Johnson et al. (1998). It involves the use of multiple thresholds and counting runs of

values above a threshold along a radial. The technique accounts for noise by incorporating a heuristic of how many successive range gates are allowed to fall below the threshold before the run is terminated. The centroid of such runs are then used as a proxy for the storms and tracked on the basis of proximity to expected position. While these heuristics work well for radar images from the NEXRAD network for which they were devised, they are not easily transferable to other types of weather imagery, or even to data from radars that are not broadly comparable to the WSR-88D. In addition, the technique of Johnson et al. (1998) involves iterating through the data set once for each threshold. Such performance is tolerable when using five thresholds on an image corresponding to a single radar scan (approximately 365x460 pixels, the problem that the Johnson et al. (1998) was intended to address), but it doesn't scale well when either the number of thresholds or the size of the image is increased.

a. Terminology

Image processing terms are explained when they are first used in this paper. For readers' convenience, quick definitions of the terms are provided below:

1. **Watershed transform**: An efficient technique for finding regions of high intensity by testing all possible thresholds in one pass through the image.

2. **Basin**: A region identified by the watershed algorithm by starting out at a local maximum.

3. **Saliency**: Criterion to check whether a region should be retained. Saliency is usually defined based on the depth of the basin. This paper modifies it to be a check on the

area of the basin.

4. **Hysteresis**: A second, lagging threshold that is usually defined as a decrement from the first threshold. In this paper, hysteresis threshold is defined as the threshold at which the basin becomes salient.

5. **Foothills**: The foothills denote the region of support for a maximum. Within this region of support, no new maxima may be found.

b. Organization

The rest of this paper describes a general purpose technique for the identification of cells in different types of weather images and demonstrates its effects on a variety of radar and satellite images. The basis of the technique, the watershed transform, is described in Section 2. The conceptual framework behind the extension of the watershed transform to enable finding storm cells in weather images is described in Section 3. The actual implementation details of the algorithm, including pointers on parameter choices, are provided in Section 4. Results of using this algorithm to identify storm cells in a variety of remotely sensed weather images are illustrated in Section 5.

2. Watershed Transform

The term *watershed*, in common geographical usage, refers to a drainage basin. The drainage basin collects all the water within the area covered by the basin, i.e., water does

not flow out of a basin. The watershed transform of Beucher and Lantuejoul (1979); Beucher (1982) borrows its conceptual model from the idea of watersheds as drainage basins divided by ridges of land. The watershed transform is a region-based object identification approach that is now the method of choice in the image processing community for identifying objects in images (Roerdink and Meijster 2001). Unlike conventional image processing transformations which rely on convolution and have frequency counterparts, the watershed transform is morphological and sequential i.e. it proceeds on a pixel-by-pixel basis based on the attributes of a pixel's neighborhood. In keeping with the terminology in most numerical and optimization methods, the watershed algorithm is normally described as a minima-finding method. Here, we'll describe it as a maxima-finding method so that the relationship to finding high-intensity storm cells is straight-forward.

Conceptually, the idea is to flood the image starting from the global maximum. The flooding level is slowly decreased so that flooding can proceed at lower and lower levels, a process called immersion. The entire area covered by water flowing from a single maximum is a termed a basin and the points where two basins meet form region boundaries (See Figure 2a). A key advantage of the watershed approach is the lack of a prespecified threshold – in effect, *all* possible thresholds are attempted.

While it is certainly conceivable to implement the simple thresholding approach at all possible thresholds,[1] simulating the immersion process would involve iterating through the entire image once for each threshold. The watershed approach was impractical for real-world applications, until Vincent and Soille (1991) described an efficient algorithm to implement

[1]When applied on digital images, there is only a finite number of candidate thresholds. These correspond to the actual data values to be found in the image.

it.

The method of Vincent and Soille (1991) implements the watershed transform efficiently by iterating through the image and forming a data structure that maps, to each digital image value, all the pixel coordinates that contain that value. The structure is then sorted in descending order of intensity values. Flooding the image at a threshold is simulated by simply processing all the pixels at a particular level. At each such pixel, all the directions in which the intensity reduces are identified and the neighboring pixel in that direction is added to the basin. All the pixels in the basin are similarly analyzed until one reaches a local minimum, where there is no direction in which to descend (See Figure 2b). The entire set of pixels accumulated starting from a single pixel is termed a basin – this corresponds to a cell.

In Vincent and Soille (1991)'s algorithm, all basins, at all flooding levels, are found in one single pass through the image. A naive implementation of a multiple thresholding scheme may yield the same result, but it is impractical to process large remotely-sensed geospatial fields in real-time by iterating through the entire image once for each threshold level.

On real-world images, the conventional watershed algorithm produces exceedingly small regions because there is a cell for each local maximum. There are two potential solutions to this problem, which in one form or another affects all cell identification methods. One approach is to smooth the image beforehand to reduce the number of spurious maxima. The second approach, introduced by Najman and Schmitt (1996), is to sequentially merge neighboring basins whose saliency is below some prespecified threshold. Najman and Schmitt (1996) defined the saliency as the difference between the maximum level and the level at the basin boundary (See Figure 2b). Practical implementations of the watershed transform

employ both these solutions (Roerdink and Meijster 2001).

The watershed transform, however, does not work on weather imagery (see Figure 3b). The image shows the result of applying the method of Najman and Schmitt (1996) with some appropriate smoothing and saliency checks on an infrared channel image from the SEVIRI satellite. As is readily apparent, the cells identified by the watershed transform look nothing like storm cells. Indeed they look like watersheds.

It has been noted (Lakshmanan et al. 2003) before that the watershed algorithm performs poorly on weather images. While a clustering approach does identify cells in a satisfactory way (See Figure 3c), it has the typical drawback of a clustering approach (Witten and Frank 2005) in that the final clusters are very sensitive to the choice of initial centers. This means that associating the clusters identified between time frames is not possible (See Figure 4). The association problem can be side-stepped by estimating motion of the clusters by finding the spatial dislocation at which the cluster's pixel values at the current frame are most correlated with the previous frame (regardless of what the clustering result was for the previous frame). While the motion estimates derived with such a method proved to be very robust (Yang et al. 2006), the drawback of not associating clusters is that extracting trends of properties of the cluster across time is not possible.

3. Extending the Watershed Transform: Conceptual Model

Why doesn't the watershed transform work on weather images? How can it be extended so that it can be used to identify storm cells on weather images?

One problem lies in the definition of saliency of a basin, as the height difference between the maximum from which water flowed and the point at which the water level meets that from another basin (See Figure 2a). This definition of saliency does not correspond to the typical understanding of a storm cell as evidenced in the work of Crane (1979) or Rosenfeld (1987). Instead, as seen in the definition of a mesoscale convective complex (Augustine and Howard 1988), a storm entity is defined as salient if it meets a certain size threshold. In other words, it's not the depth of the basin, but the areal extent of the basin that counts. Thus, the first change to the conceptual idea behind the watershed technique is to redefine the saliency to be the areal extent of the basin, rather than the height from which the water has flowed. This is shown in Figure 5a. It should be noted that this saliency criterion leads to early stopping of the basin creation process, as in the first basin of Figure 5b. Thus, the size threshold chosen for saliency can lead to cells that are smaller than would have been realized if the immersion process had been carried out completely.

The watershed technique appears, at first glance, to incorporate multiple thresholds which are local, not global, because a basin is defined in terms of the level at which it starts to get flooded. Different basins do have different starting levels. However, a basin is stopped either when the water level meets that of another basin or the value falls below a threshold shown by the dashed line at the bottom of the intensity plot in Figure 5a. This threshold is the

one that corresponds to the threshold level of a simple thresholding scheme such as the one in Figure 1a. So, instead of defining a global minimum threshold, it is necessary to define the minimum threshold as a hysteresis level. The extension of the watershed transform with a hysteresis threshold is shown in Figure 5b.

By defining the minimum threshold to be a hysteresis level, rather than a global one, basin mixing can happen, where points that would have been within the basin defined by one maximum fall into a basin defined by a secondary maximum simply because the basin creation was stopped. To avoid this problem, it is necessary to define a region of support for each maximum (we'll call them *foothills*, see Figure 5c). This region of support is larger than the basin itself, but consists of points that should not be assigned to a different basin.

It is tempting to define the hysteresis level to correspond broadly to the idea espoused by Crane (1979), of defining a cell in terms of a local maximum and a second threshold defined in terms of being a certain intensity level (3dBZ in the case of the radar reflectivity images used by Crane (1979)) below that local maximum. However, there is no guarantee that basins created using such a definition will meet the saliency check. Recall that we have modified the saliency definition to correspond, not to the height of the basin, but to the area. Thus, the hysteresis level also has to be redefined as the level at which the size of the basin meets the saliency criteria. To avoid noise contamination from spurious peaks, it is necessary to place an upper limit on the depth as well. Defining the hysteresis level in terms of areal extent is shown in Figure 5d.

4. Implementation of Extended Watershed Transform

The conceptual framework behind the extension of watershed algorithm used in this paper was described in Section 3. In this section, we will describe the stages of the algorithm as it is implemented, the parameters that the user needs to specify and provide pointers on how to choose those parameters.

The stages of the algorithm are shown in Figure 6. First, the input image is smoothed to reduce the occurence of spurious peaks. Then, the image is quantized and transformed to a data structure that maps intensity level to all the pixels at that level. The data structure is sorted and centers (the points from which flooding will commence in the conceptual model) identified. Cells (basins in the conceptual model) are then identified, taking the hysteresis level and saliency checks into account.

a. Smoothing

The use of a saliency criterion that is a combination of depth and distance helps to avoid defining basins based on short or narrow maxima. However, smoothing the image before performing the watershed algorithm is still useful. This is because, as shown in the top row of Figure 7, spurious peaks that are part of a valid basin do change the definition of that basin. In order to achieve stable cell identification, it is important to smooth the images beforehand. Secondly, smoothing reduces the number of centers to be considered when trying to determine which maximum a pixel would have been flooded by, thereby increasing the efficiency of the foothills stage.

Smoothing provides an opportunity to set the scale at which storms are identified. For

example, by smoothing images over large neighborhoods, it is possible to look for mesoscale systems and avoid stormscale entities. However, as will be discussed shortly, scale is better set using the saliency criteria. Thus, care should be taken to ensure that the scale at which smoothing is carried out corresponds to one that will maintain basins of the size that would be expected on the basis of the saliency criteria.

Any smoothing filter may be used, but different smoothing filters provide better results on different types of images. For example, a rank-based filter [2] is better on images with speckle noise while an oriented filter is better for processing entities on the scale of squall lines (Lakshmanan 2004). A small-scale Gaussian filter is a good general-purpose filter because of its superior space-frequency properties (Jain 1989) and can be used when there are no other over-riding considerations.

b. Quantization

After smoothing, the image pixels need to be quantized. Image values can not be retained as floating point numbers because the efficiency of the watershed algorithm derives from a data structure that provides quick and random access to all the pixels at a particular data value. In order to implement this data structure, the pixel values need to be integers. The

[2] A rank-based filter is a filter that sets a pixel's value based on the sorted values of its neighbors. The most commonly used rank-based filter is the median filter, where the output is the 50^{th} percentile value within a specific neighborhood. Percentile values greater than 50% lead to dilation of storm entities and values less than 50% lead to erosion of storm entities.

image values can be linearly scaled using:

$$Q_{xy} = round(\frac{I_{xy} - a}{\delta}) \tag{1}$$

to scale image intensity values I_{xy} to quantized values Q_{xy}. The *round* function will round the fraction provided to the nearest integer and the parameters a and δ will vary depending on the type of image.

It's desirable to place upper and lower bounds on the value of Q_{xy}, to limit the size of the data structure. The quantization function then becomes:

$$Q_{xy} = \begin{cases} 0 & \forall I_{xy} \leq a \\ round(\frac{I_{xy}-a}{\delta}) & \forall a < I_{xy} \leq b \\ round(\frac{b-a}{\delta}) & \forall I_{xy} > b \end{cases} \tag{2}$$

(See Figure 7c). The quantity $round(\frac{b-a}{\delta})$ will be referred to as the *maxlevel* in the rest of this section.

Note that this quantization step can be used to change the problem of finding minima in images such as infrared temperature into one of finding maxima. The δ simply needs to be negative in such a case, and $a > b$:

$$Q_{xy} = \begin{cases} round(\frac{b-a}{\delta}) & \forall I_{xy} \leq b \\ round(\frac{I_{xy}-a}{\delta}) & \forall b < I_{xy} \leq a \\ 0 & \forall I_{xy} > a \end{cases} \tag{3}$$

(See Figure 7d).

Large values of δ can be used to reduce the dynamic range in images. This is useful if the instrument tends to yield noisy data, but where the spatial resolution is too poor for

spatial smoothing to be employed for noise reduction.

c. Transformation

The quantized values are now placed into a data structure that enables efficient simulation of the immersion process:

Procedure 1 Create data structure
Require: $Q_{xy}, maxlevel$

1: $pixels \leftarrow$ list of size maxlevel
2: **for** $level = 0$ to $maxlevel$ **do**
3: $\quad pixels[level] \leftarrow$ empty list
4: **for all** pixels x, y in Q **do**
5: $\quad$ add x, y to $pixels[Q_{xy}]$

The rest of the algorithm iterates through this data structure, not through the image. The quantized image is still needed for capturing the basin, however.

d. Finding Centers

The next step is to find all the candidate local maxima. The list of centers can be a subset of the list of pixels – it is not necessary to perform the full algorithm at pixels that are proximate to a local maximum because these pixels will either be part of that maximum's basin or its foothills. Thus, the subset of *pixels* that need to be considered as maxima can be obtained by iterating through the *pixels* in reverse order of intensity and removing from the list neighbors of those *pixels* which are candidate centers. However, the algorithm may

be implemented, at the cost of some efficiency, without doing this pre-pruning by merely initializing *centers* to a copy of the *pixels* data structure.[3].

e. Immersion Simulation

The output of the algorithm is a labeled image, where each pixel's value is the basin that it belongs to. Pixels that are not part of any basin (storm cell) will be assigned a basin number of zero. First, all the pixels in the labeled image, B (for basin), are initialized to a negative number. Then, the immersion simulation of the extended watershed algorithm is carried out by iterating through the *centers* data structure (See Procedure 2).

Note that *hlevel* is slowly decreased (with increasing depth) so that the basin is grown only until it meets the saliency check. Capturing a center involves growing the basin starting at the center and capturing all points above the *hlevel* that would be immersed with water flowing from the center (See Procedure 3).

Reserving all the foothills also involves region growing starting at the center and capturing all points that are below the *hlevel* and to which the current center is the closest of all centers. The implementation is very similar to Procedure 3 except that in addition to the threshold check on value, there needs to be another check, this time on the distance between the pixel xy and each *center*. Note that this distance needs to be geodesic (i.e. in the space of the image and including only those pixels that are greater than a). This is because the foothills of a basin should include only those pixels to which the basin is connected. As a

[3]In a two-dimensional image, there are eight neighboring pixels around each local maximum, so pre-pruning will lead to at least a eight-fold increase in the efficiency of the immersion simulation stage

Procedure 2 Find basins

Require: $maxlevel, maxdepth \leq maxlevel, B$

Require: $pixels[level], centers[level]\ \forall\ level$ such that $0 \leq level \leq maxlevel$

```
1: basinNumber ← 1
2: for all pixel in B do
3:     B_pixel ← -1
4: for depth = 0 to maxdepth do
5:     for level = maxlevel to 0 step −1 do
6:         hlevel ← level − depth
7:         for all center in centers[level] do
8:             if B_center < 0 then
9:                 capture basin starting at center
10:                if basin was captured then
11:                    reserve foothills for center
12:                    increment basinNumber
13:                else
14:                    add center to centers[level − 1] to process center at next lower
                       level
15:        Set foothill points to background basin
```

fast approximation, the Euclidean distance may be used, and the geodesic distance verified only for points that are within that Euclidean distance.

Procedure 3 Capture basin

Require: $hlevel, saliency, center, Q, basinNumber, B$

$neighbors \leftarrow$ empty stack
$foothills \leftarrow$ empty stack
$basin \leftarrow$ empty list
add $center$ to $neighbors$
repeat
    $pixel \leftarrow neighbors_{next}$
    add $pixel$ to $basin$
    for all xy contiguous to $pixel$ **do**
        if $Q_{xy} \geq hlevel$ **then**
            add xy to $neighbors$
        else
            add xy to $foothills$
until $neighbors$ is empty
if $size(basin) < saliency$ **then**
    Basin has not been captured
    $foothills \leftarrow$ empty stack
    $basin \leftarrow$ empty stack
else
    for all $pixel$ in $basin$ **do**
        $B_{pixel} \leftarrow basinNumber$

f. How Scale Factors

The size of the cells detected by the extended watershed technique can be affected in two ways. Short and narrow peaks can be smoothed away by spatial filtering of the image prior to doing the immersion simulation. Thus, for example, smoothing the image with a filter with large spatial support (a large σ value) will lead to rounded peaks and larger basins. The direct means of affecting the scale is to set the saliency threshold appropriately. The saliency in the technique of this paper is the minimum spatial extent of a basin before it is regarded as a valid storm cell. By increasing the saliency, we can choose retain only those storms that have the required spatial scale (See Figure 8). Note also that the early stopping provided by the saliency criterion causes the technique to behave more like a centroid-finding technique at small scales (Figure 8d) and as a complete storm identification technique at larger scales (Figure 8c).

How cells smaller than the saliency threshold should be treated depends on whether smaller, but contiguous, cells should be combined into larger lines and fronts. Recall that the hysteresis level is defined in terms of the maximum depth at which the saliency threshold for area can be met. By decreasing the hysteresis level, smaller storms can be combined to create larger entities. Thus, to detect squall lines (where it is to be expected that the area between small cells has low intensity values), the saliency area threshold would be set high but the hysteresis level would be lowered. That is the algorithm presented in this paper. To avoid such merging of smaller cells into larger entities, the hysteresis level could be set to a prespecified decrement from the threshold level, and not allowed to be lowered below that. Preliminary analysis of doing this was not enouraging – it appears that basin merging

is required to match human perceptions of what a valid storm cell is (See Figure 9c).

It is possible to implement hierarchical storm detection by saving all the basins that meet the saliency criteria at each hysteresis level. Basins at a high hysteresis level are all contained within basins at any lower hysteresis level.

Note that while scale can be affected either by smoothing the image or by setting the saliency threshold, methods such as wavelet analysis can not be used. Wavelets are a multi-resolution method; the technique introduced in this paper needs to operate at the original resolution of the image.

g. Associating and Tracking Storms

Often, the main purpose of identifying storms in radar or satellite images is to track them across time. By tracking storms across time, it is possible to retrieve trends in storm properties and use these in nowcasting. While such tracking is not a focus of this paper, it is important to demonstrate that tracking is possible when storm cells are identified using the method described in this paper.

The major problem to be solved when tracking storms across time is to determine, for each storm in the previous image, the storm in the current image with which it is associated with. This is a difficult problem because storms change with time. They may also split or merge with other storms. The method of carrying over properties of storms when storms split or merge also needs to be determined.

One heuristic for association, used by Johnson et al. (1998), is to project the location of every storm's centroid based on its past movement and to then associate every storm in the

previous image with the storm in the new image whose centroid is closest to that projected centroid. Another heuristic, used by Morel et al. (1997), is to associate storms based on the degree of overlapping pixels. Neither heuristic works well if the storms move or change a lot between images such as if the temporal gap between images is large or if the spatial resolution of the images is poor.

A somewhat better approach is that of Dixon (1994) where storm association is treated as an optimization problem. Long-lived, larger and more intense storms should be retained as much as possible. In addition, storms should be associated with the closest storm (as measured by the inter-centroid distance) and with the storm with which there is considerable overlap. The cost function used could be a weighted sum of all of these utility functions, but the choice of the appropriate weights would have been heuristic and not easily transferred between different types of weather images. For simplicity, we used a greedy optimization approach that maximized the utilities in the above mentioned order. Once associated, the storm movement was estimated using a constant-acceleration Kalman filter model (Kalman 1960; Brown and Hwang 1997).

5. Results

The storm cell identification method introduced in this paper was applied to several types of remotely sensed images.

a. NEXRAD

Radar reflectivity data from the NEXRAD network are combined in real-time to create a 3D mosaiced dataset that covers the coterminous United States (CONUS) at a resolution of approximately $1km \times 1km \times 1km$ (Lakshmanan et al. 2006). The effect of applying the technique of this paper to the reflectivity composite derived from that 3D mosaic is demonstrated in Figure 9.

The parameter values used are shown in Table 1. The saliency threshold should be chosen depending on the scale at which storm identification is desired and whether or not multi-cell clusters are permissible. The radar data are quality controlled (Lakshmanan et al. 2007) as part of the data fusion process. In that stage, artifacts due to anamolous progragation and sunstrobes are removed. Thus, a relatively light hand in terms of smoothing suffices for this data set.

The technique takes $13\mu s$ of CPU time (0.6 seconds of clock time) to process a 3000x6000 pixel image using a 1GHz AMD Opteron processor.

b. CASA

The Collaborative Adaptive Sensing of the Atmosphere (CASA) network presently consists of four small, low-cost, low-power X-band radars in Southwestern Oklahoma. Data from those radars are combined in real-time and the cells identified using the technique of this paper (See Figure 10) are used as input to a meteorological commmand and control unit that adapatively scans the atmosphere (Brotzge et al. 2005).

The CASA data are characterized by extremely high resolution with the range gates

being $0.05km \times 1.8^o$. The pixel size in the merged radar grid is chosen to be $0.1km \times 0.1km$, similar in scale to the average radar gate sizes. However, the CASA data are subject to significant ground clutter problems because the CASA network (unlike the NEXRAD one) was designed to scan the lower atmosphere $(0 - 3km)$ and because throrough quality control has not been applied to the CASA reflectivity data. Thus, an aggressive rank filter was used in the smoothing stage and a high saliency threshold of $2.5km^2$ (corresponding to 250 pixels) was applied (See Table 1).

c. GOES

The extended watershed algorithm described in this paper was applied to one-minute interval scans of the 11μ infrared channel from the Geostationary Operational Environmental Satellite (GOES-12 Eastern sector) on Oct. 12, 2001 (See Figure 11). The spatial resolution of the data was approximately $4km \times 4km$. Compared to the radar data, the spatial resolution of the satellite data is significantly poorer. Thus, storm cells are extracted at somewhat larger scales than is possible using radar data. Even a saliency threshold of $160km^2$ (See Table 1) corresponds to a mere 10 pixels in the image. Also, no smoothing filter was applied because the infrared data are already quite clean and smoothing would further degrade the effective spatial resolution of the data.

d. SEVIRI

The algorithm was also applied to infrared brightness count data from the Meteosat-8 Spinning Enhanced Visible and Infrared Imager (SEVIRI) satellite. The SEVIRI satellite

has imaging capabilities similar to the Advanced Baseline Imager (ABI) that will be deployed on board the GOES-R.

The infrared (11μ) channel data used were from Jan. 5, 2005 and were collected at 15-minute intervals. The spatial resolution was approximately $2.7km \times 2.7km$. Because of the higher resolution than GOES, it was possible to employ a Gaussian filter at the smoothing stage. As with the GOES data, the saliency thresholds had to be higher so as to obtain the storm cores (See Figure 12). The dynamic range of the SEVIRI data is much higher than that of GOES. However, because of the relatively poor spatial resolution (as compared to, say, NEXRAD), the high variance can not be addressed by spatial smoothing alone. Therefore, a higher δ was used (See Table 1). The impact of not using a higher δ is shown in Figure 12c – note the large numbers of spurious cells that still do meet the saliency criteria.

e. Summary and Conclusion

The underlying ideas in storm cell identification have not changed since the seminal papers of Crane (1979) and Rosenfeld (1987). Because these methods are too simplistic to work in practice, operational storm cell identification methods such as those of Johnson et al. (1998), Dixon (1994) or Augustine and Howard (1988) have relied on a set of heuristics. The heuristics of each of the above techniques are tuned to the particular dataset they were applied to and can not be easily applied to other types of meteorological data. Furthermore, these methods rely on multiple passes through the image data and therefore do not scale to high resolution or large data sets as produced by CASA, mosaiced NEXRAD or SEVIRI. This paper thus pointed the need for a sophisticated, efficient technique that would work on

a variety of weather imagery.

The watershed transform of Vincent and Soille (1991) and the improvements made by Najman and Schmitt (1996) were introduced as the most popular object identification technique. The popularity stems from two reasons: (1) the watershed algorithm tests all possible thresholds removing the need to define a threshold to identify objects and (2) the algorithm can be implemented in a single pass through the image. For several reasons, pointed out in detail in the paper, the formulation of the watershed transform does not apply well to the problem of finding storm cells. Hence, we adapted and extended the watershed algorithm to the storm cell problem. This involved changing the saliency criterion from the one proposed by Najman and Schmitt (1996), introduction of hysteresis into the watershed algorithm, making the hysteresis level dependent on the saliency and finally the use of a concept that we called foothills to avoid basin contamination.

The paper also provided the implementation details of the extended watershed algorithm. Like the conventional watershed transform, the method described in this paper relies on a single pass through the image to achieve cell identification at all possible thresholds within some practical quantization bounds. The implementation yields a robust, fast algorithm that is capable of processing an image with 18 million pixels in a fraction of a second on a conventional workstation.

The algorithm was demonstrated on a variety of radar and satellite imagery. Good choices for the parameters for the enhanced watershed algorithm were also discussed. In particular, we demonstrated performance on high-resolution, large scale radar reflectivity fields (mosaiced NEXRAD), extremely high-resolution, but very noisy radar reflectivity fields (mosaiced CASA), coarse resolution infrared temperature satellite channel (GOES)

and moderate resolution, global infrared temperature satellite channel (SEVIRI). Parameter choices for each of these cases were described, and it was shown that the extended watershed technique successfully identified storms on all these fields.

This paper presents a formal, efficient way of finding regions where a remotely sensed field's values are greater (or lesser) than a locally varying threshold. If the colder temperatures in infrared temperature correspond to ground or higher dBZ values in radar reflectivity correspond to anamolous propagation, the identified entities will not be storms. In practice, the technique of this paper should be used to identify storm candidates, and the overall context used to determine whether the identified candidates are indeed storms.

Acknowledgements

Funding for this research was provided under NOAA-OU Cooperative Agreement NA17RJ1227, Engineering Research Centers Program (NSF 0313747). We acknowledge Dr. Robert Kuligowski of NESDIS and Dr. John Moses of NASA for their assistance with the satellite data.

The extended watershed algorithm described in this paper has been implemented within the Warning Decision Support System Integrated Information (WDSSII) as the w2localmax algorithm. It is available for download at www.wdssii.org.

REFERENCES

Augustine, J. and K. Howard, 1988: Mesoscale convective complexes over the United States during 1985. *Mon. Weather Rev.*, **116 (3)**, 685–701.

Beucher, S., 1982: Watersheds of functions and picture segmentation. *Proc. IEEE Int. Conf. Acoustics, Speech and Signal Proc.*, Paris, 1928–1931.

Beucher, S. and C. Lantuejoul, 1979: Use of watersheds in contour detection. *Proc. Int. Workshop Image Proc., Real-Time Edge and Motion Detection/Estimation*, Rennes, Fr.

Brotzge, J., D. Westbrook, K. Brewster, K. Hondl, and M. Zink, 2005: The meteorological command and control structure of a dynamic, collaborative, automated radar network. *21st Int'l Conf. on Inter. Inf. Proc. Sys. (IIPS) for Meteor., Ocean., and Hydr.*, San Diego, CA, Amer. Meteor. Soc., 19.15.

Brown, R. and P. Hwang, 1997: *Introduction to Random Signals and Applied Kalman Filtering*. John Wiley and Sons, New York.

Crane, R., 1979: Automatic cell detection and tracking. *IEEE Trans. on Geoscience Electronics*, **17**, 250–262.

Dixon, M., 1994: Automated storm identification, tracking and forecasting – a radar-based method. Ph.D. thesis, University of Colorado and National Center for Atmospheric Research.

Jain, A., 1989: *Fundamentals of Digital Image Processing*. Prentice Hall, Englewood Cliffs, New Jersey.

Johnson, J., P. MacKeen, A. Witt, E. Mitchell, G. Stumpf, M. Eilts, and K. Thomas, 1998: The storm cell identification and tracking algorithm: An enhanced WSR-88D algorithm. *Weather and Forecasting*, **13 (6)**, 263–276.

Kalman, R., 1960: A new approach to linear filtering and prediction problems. *Trans. ASME – J. Basic Engr.*, 35–45.

Lakshmanan, V., 2004: A separable filter for directional smoothing. *IEEE Geosc. and Remote Sensing Letters*, **1 (3)**, 192–195.

Lakshmanan, V., A. Fritz, T. Smith, K. Hondl, and G. J. Stumpf, 2007: An automated technique to quality control radar reflectivity data. *J. Applied Meteorology*, **46 (3)**, 288–305.

Lakshmanan, V., R. Rabin, and V. DeBrunner, 2003: Multiscale storm identification and forecast. *J. Atm. Res.*, **67**, 367–380.

Lakshmanan, V., T. Smith, K. Hondl, G. J. Stumpf, and A. Witt, 2006: A real-time, three dimensional, rapidly updating, heterogeneous radar merger technique for reflectivity, velocity and derived products. *Weather and Forecasting*, **21 (5)**, 802–823.

Morel, C., F. Orain, and S. Senesi, 1997: Automated detection and characterization of MCS using the meteosat infrared channel. *Proc. Meteor. Satellite Data Users Conf.*, Eumetsat, Brussels, 213–220.

Najman, L. and M. Schmitt, 1996: Geodesic saliency of watershed contours and hierarchical segmentation. *IEEE Trans. Patt. Anal. and Mach. Intell.*, **18**, 1163–1173.

Rinehart, R. and E. Garvey, 1978: Three-dimensional storm motion detection by conventional weather radar. *Nature*, **273**, 287–289.

Roerdink, J. and A. Meijster, 2001: The watershed transform: Definitions, algorithms and parallelization strategies. *Fundamenta Informaticae*, **41 (3)**, 187–228.

Rosenfeld, D., 1987: Objective method for analysis and tracking of convective cells as seen by radar. *Journal of Atmospheric and Oceanic Technology*, **4 (3)**, 422–434.

Tag, P., R. Bankert, and L. Brody, 2000: An AVHRR multiple cloud-type classification package. *J. Appl. Meteor.*, **39**, 125–134.

Vincent, L. and P. Soille, 1991: Watersheds in digital spaces: An efficient algorithm based on immersion simulations. *IEEE Trans. on Patt. Anal. and Mach. Intell.*, **13 (6)**, 583–598.

Witten, I. and E. Frank, 2005: *Data Mining*. Elsevier, 524 pp.

Yang, H., J. Zhang, C. Langston, and S. Wang, 2006: Synchronization of multiple radar observations in 3-d radar mosaic. *12th Conf. on Aviation, Range and Aerospace Meteo.*, Atlanta, GA, P1.10, CD–ROM.

List of Figures

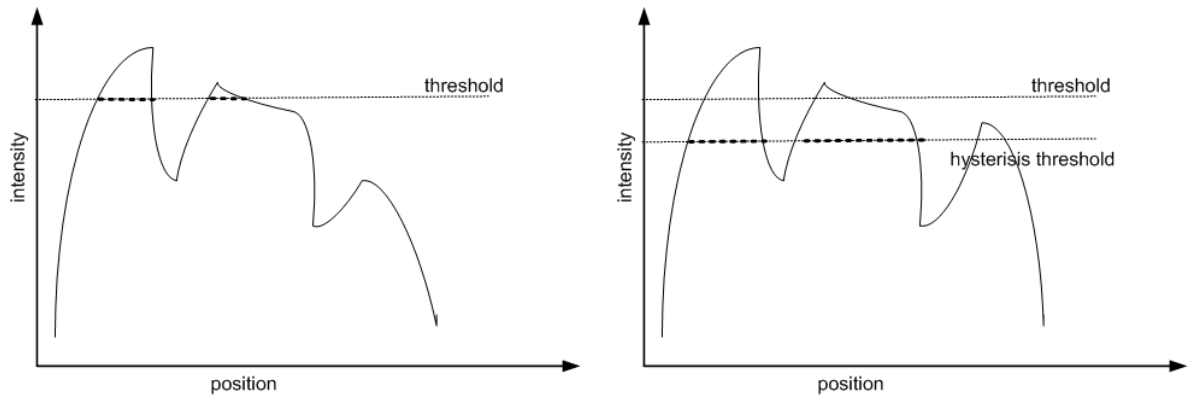

(a) (b)

FIG. 1. Thresholding with hysteresis. (a) The basic technique involving the use of a global threshold works only for mature cells that have many points above the threshold. The second cell appears very small and can be easily assumed to be noise. (b) Employing two thresholds, a high one to identify potential storms and a lower hysteresis threshold within which to continue to grow the region can capture growing cells while remaining noise-tolerant. Thus, the second cell is now captured, but the third is rightly ignored.

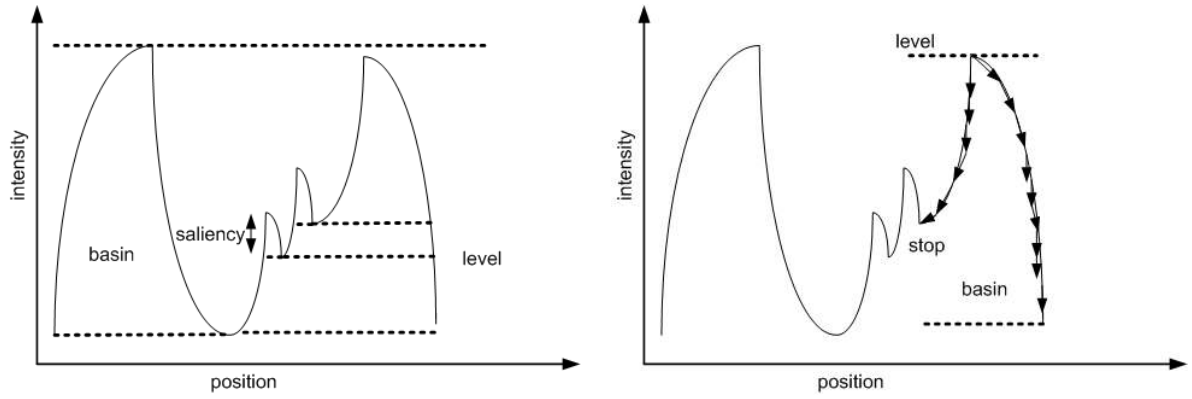

(a) (b)

FIG. 2. The watershed transform. (a) Conceptually, the idea is to flood the area one level at time, starting from the global maximum and to term all the area covered by water from the same maximum a basin. (b) Starting at a pixel at the flooding level, neighbors in a direction of decreasing intensity levels are added to the basin.

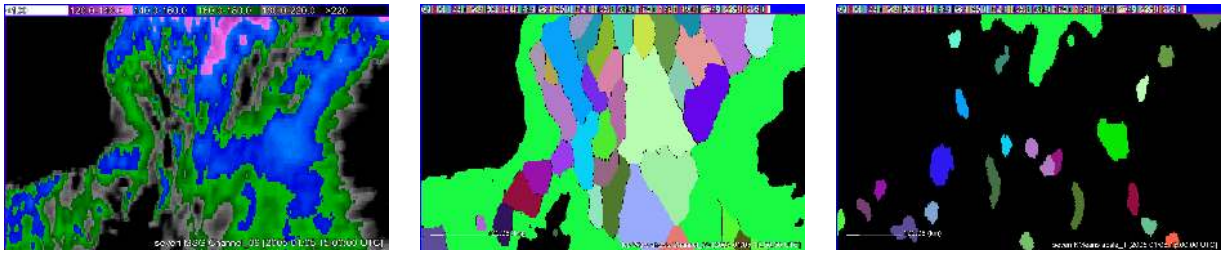

(a) (b) (c)

FIG. 3. The watershed algorithm does poorly when applied to weather images. (a) Infrared channel 9 (11-micron) image from the SEVIRI satellite. The image is over the North Sea from Jan 5, 2005 and depicts an area of approximately $600km \times 400km$. (b) Cells identified by the watershed algorithm. The colors have no significance beyond providing a way to distinguish between different cells. (c) The multiscale clustering approach of Lakshmanan et al. (2003) does well, but has the disadvantage of it not being possible to extract trends of these clusters. This is because clustering is sensitive to the initial starting point. See also Figure 4.

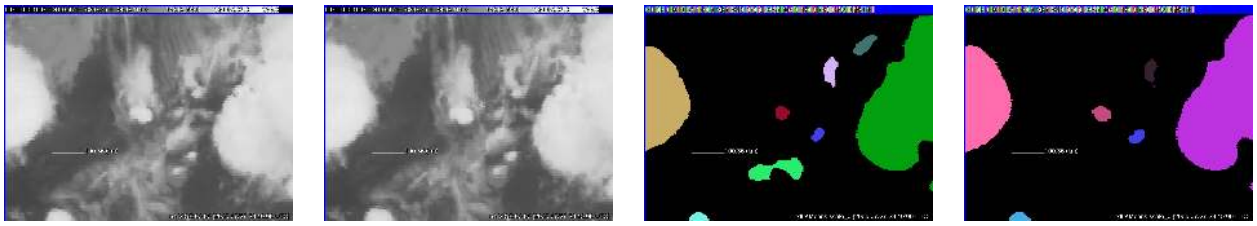

(a) (b) (c) (d)

FIG. 4. Clustering techniques identify valid cells, but are very sensitive to starting points. (a) GOES Band-4 data from July 27, 2005. The area shown covers an area of about $600km \times 400km$ centered over Arkansas. (b) Data from 5 minutes later. Note that nothing much has changed. (c) Cells identified at the most detailed scale at the first time step. (d) Cells identified five minutes later. Note the drastic difference – several of the cells identified in the previous time frame are not identified at the current one even though the input images are nearly the same. It is not possible to track cells across time if the identification process is so sensitive.

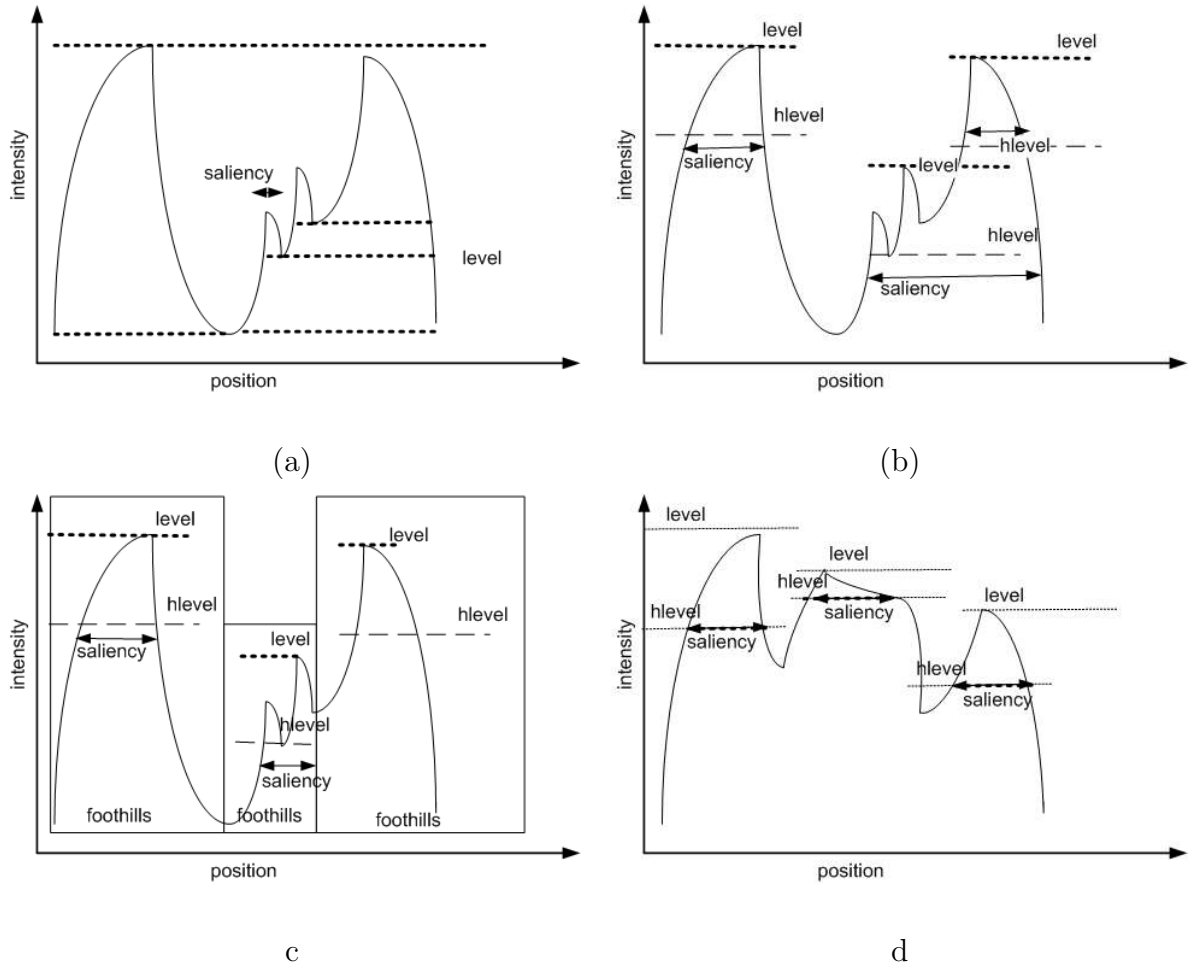

FIG. 5. Extensions to the basic watershed algorithm so that it can be used to detect storm cells in weather images. (a) The saliency needs to be defined in terms of areal extent, rather than the depth of the basin. (b) The minimum threshold of the basins should not be global, but should instead be a hysteresis level (*hlevel* in the figure). (c) While the basin is defined in terms of hysteresis level and saliency, a larger region of support, termed foothills, needs to be defined. (d) The hysteresis level needs to be defined in terms of areal extent subject to a maximum depth.

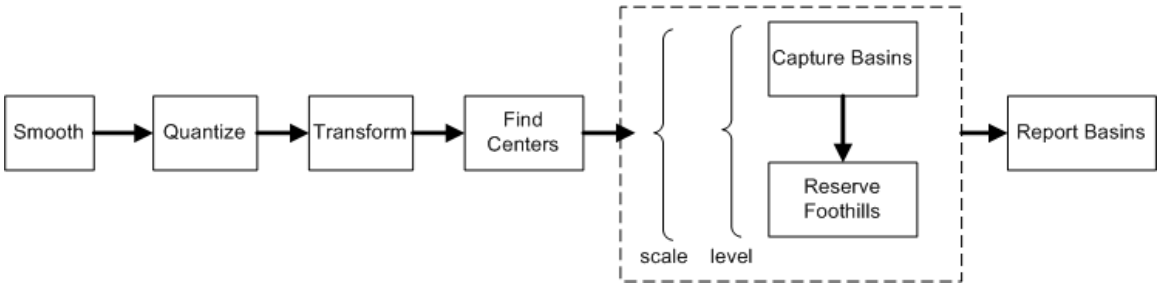

FIG. 6. Stages in the implementation of the cell identification algorithm. The dashed box is the stage where immersion is simulated while the transformation stage is responsible for the efficiency of the method. The immersion stage consists of two iterations through a data structure: one through all the scales and the other through all the levels.

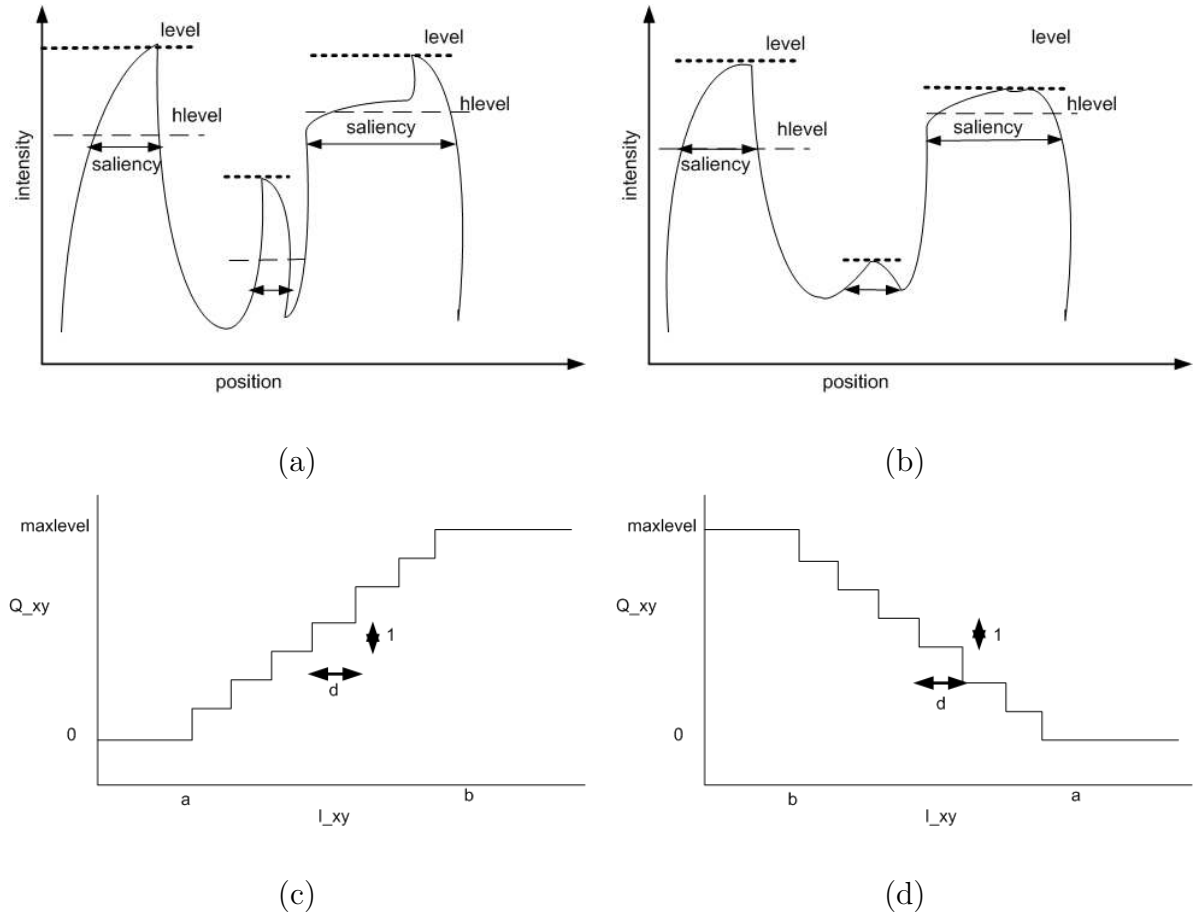

FIG. 7. (a) The saliency criteria prevent basins being formed because of narrow or short peaks such as the second peak in the figure. However, spurious peaks like the third that occur in a valid basin cause the basin boundaries to be badly defined. (b) Smoothing the image before performing the exhanced watershed algorithm makes the basins cleaner. (c) Quantization function makes the values integers so as to take advantage of the efficiency of the watershed transform (d) Quantization can be used to transform the image values, so as to look for cells defined by colder values in fields such as satellite infrared temperature.

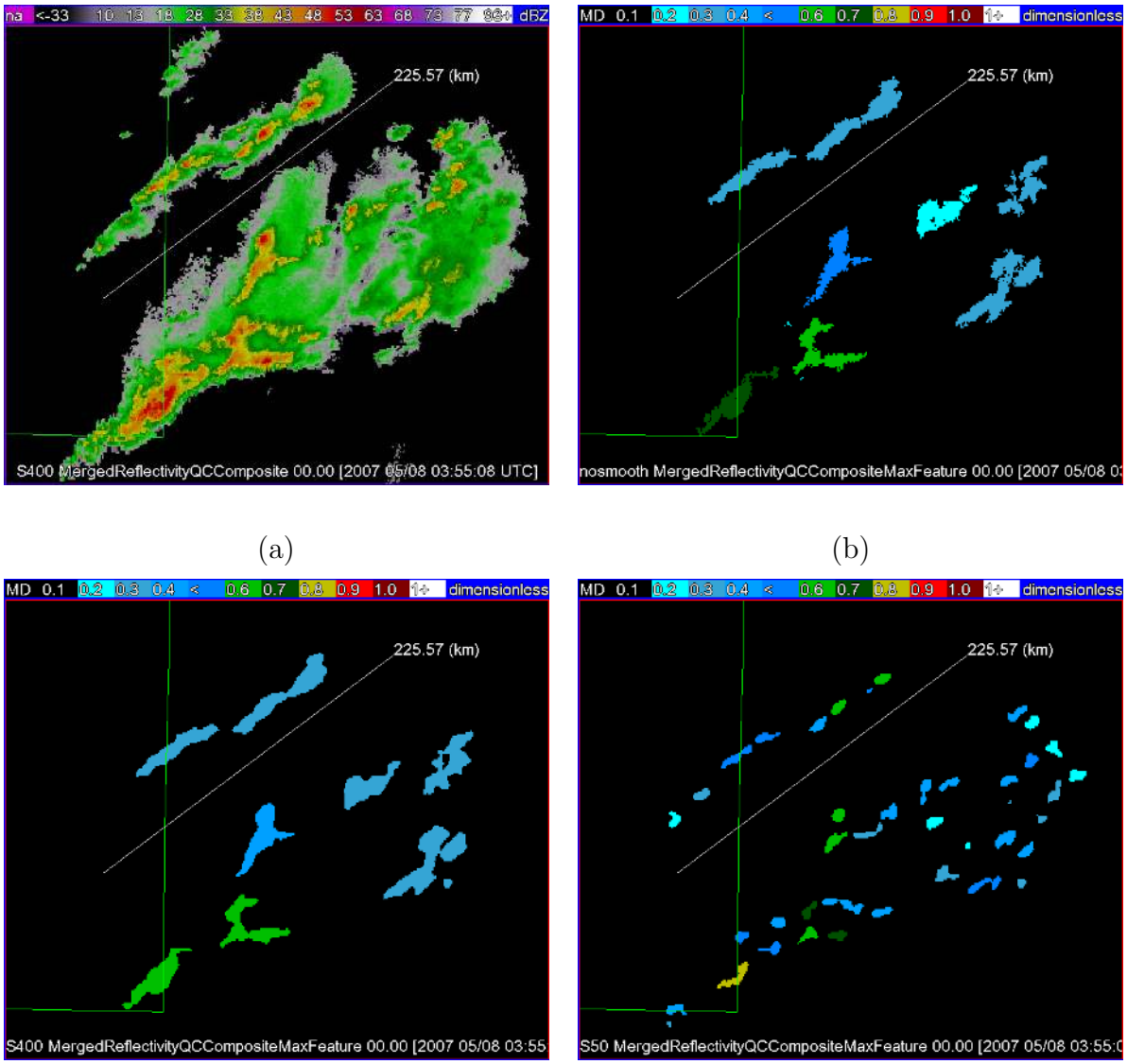

(a) (b)

(c) (d)

FIG. 8. Affecting the scale at which storms are identified using the technique of this paper through smoothing and/or saliency. (a) Input multi-radar reflectivity composite image covering an area of approximately $300km \times 300km$ over the Texas panhandle on May 8, 2007. (b) No smoothing; saliency of $400km^2$ (c) Smoothed using a Gaussian filter of $sigma = 3km$; saliency of $400km^2$ (d) Smoothed using a Gaussian filter of $sigma = 3km$; saliency of $50km^2$

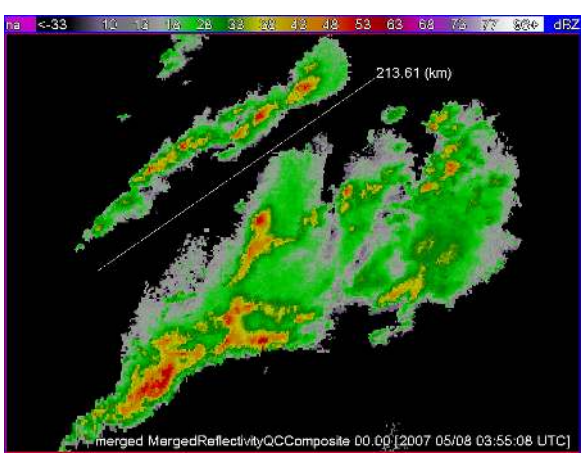

a

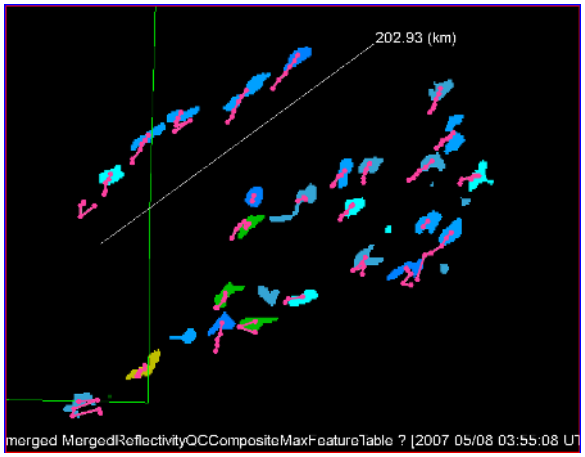

b

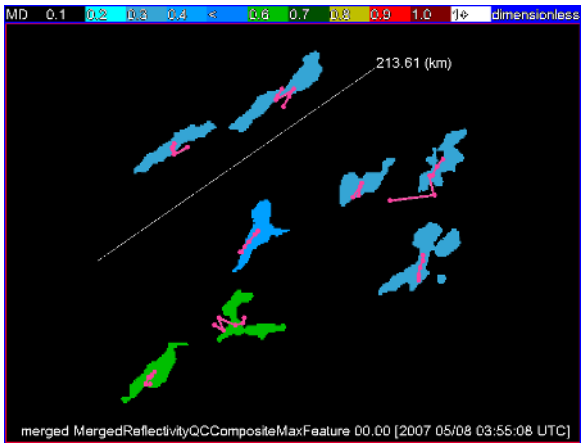

c

FIG. 9. The extended watershed algorithm of this paper applied to a multi-radar reflectivity composite image. The image covers an area of approximately $300km \times 300km$ over the Texas panhandle and comes from May 8, 2007. (a) Radar reflectivity. (b) Cells identified at a saliency of $100km^2$. The positions of the cells as they are tracked are shown superimposed on the image. (c) Cells identified at a saliency of $400km^2$. Note that smaller cells have been combined into larger entities to meet the saliency criterion.

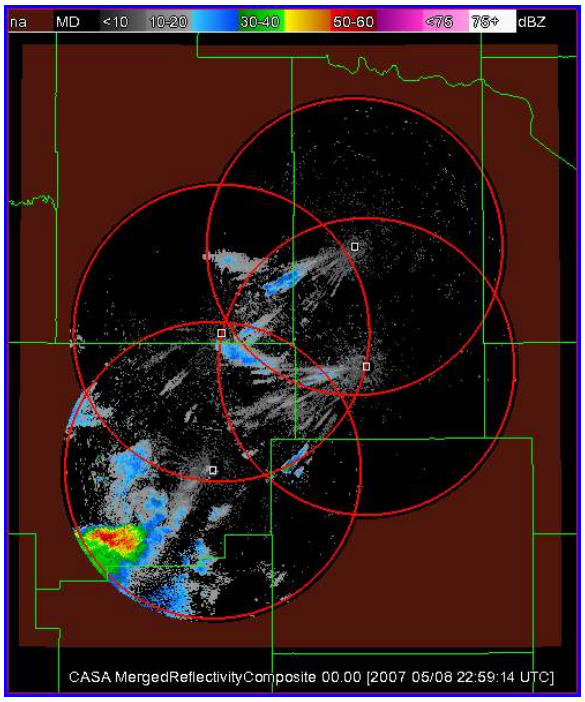

(a)

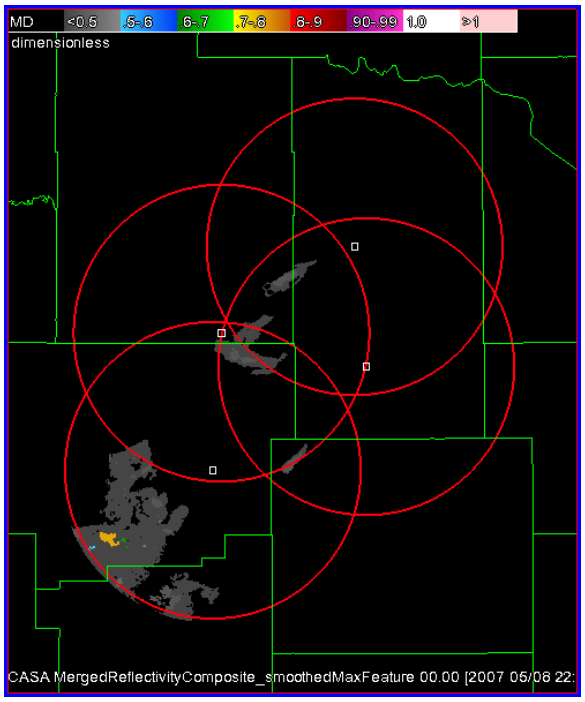

(b)

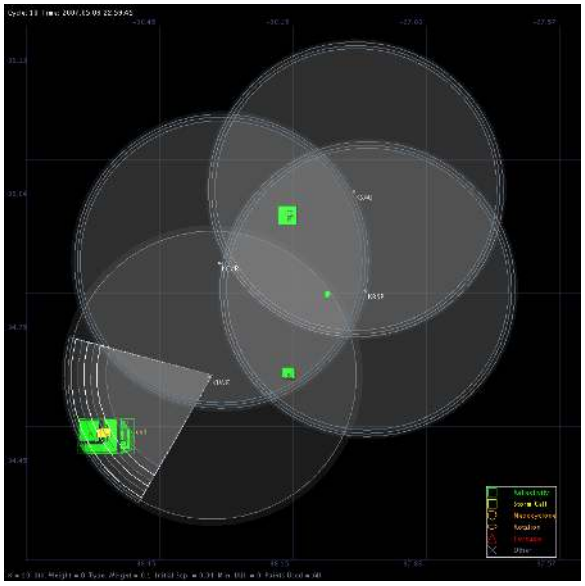

(c)

FIG. 10. The extended watershed algorithm of this paper applied to a reflectivity composite image from the CASA network. The image covers an area of approximately $120km \times 120km$ over Oklahoma and comes from May 8, 2007. (a) Radar reflectivity. The rings denote the ranges of the four CASA radars used in creating this mosaic. (b) Cells identified (in yellow) with the foothillls denoted in gray. Note that even though the data are noisy, the aggressive smoothing and saliency settings of Table 1 help reduce the impact of the noise. (c) Identified

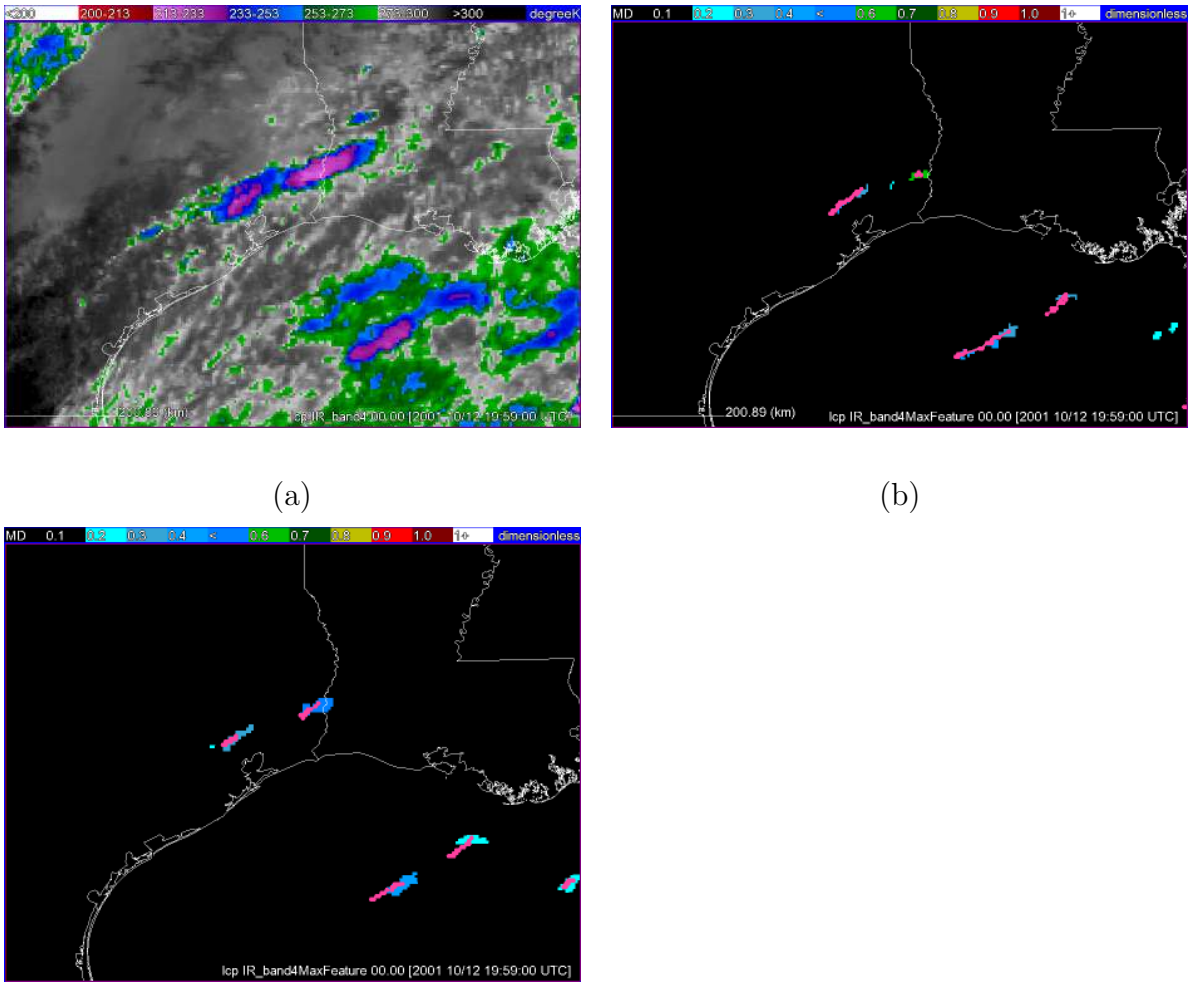

(a) (b)

(c)

FIG. 11. The extended watershed algorithm of this paper applied to a GOES-12 11μ infrared image. The image covers an area of approximately $4000km \times 2500km$ over the Gulf of Mexico and comes from Oct. 12, 2001. (a) Infrared channel. (b) Cells identified at a saliency of $160km^2$. The positions of the cells as they are tracked are shown superimposed on the image. A clustering technique (See Figure 4) is not consistent enough to provide such tracks. (c) Cells identified at a saliency of $500km^2$.

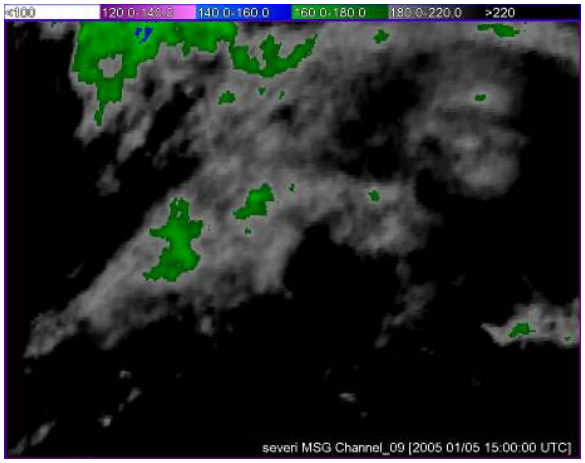

(a)

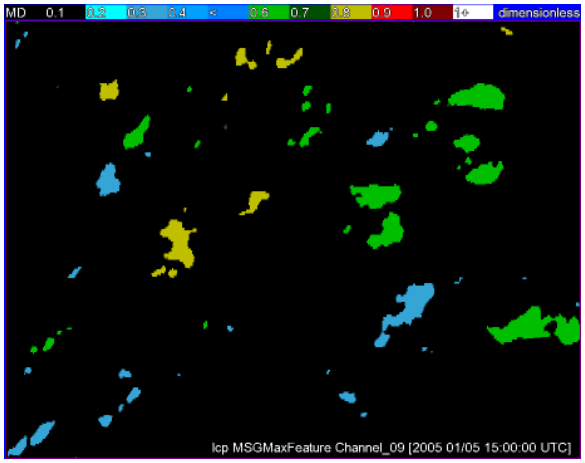

(b)

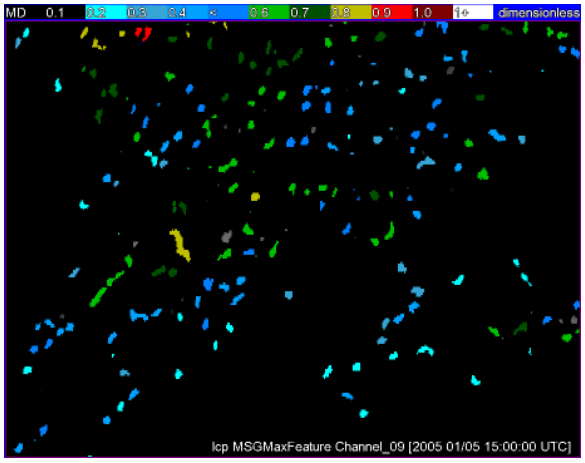

(c)

FIG. 12. The extended watershed algorithm of this paper applied to a SEVIRI infrared image. The image covers an area of approximately $1000km \times 750km$ over Northern Europe and comes from Jan. 5, 2005. (a) Infrared 11μ channel. (b) Cells identified at a saliency of $160km^2$ and $\delta = -20K$. The cells are colored on an intensity scale based on the minimum IR temperature within the cell. (c) Impact of choosing $\delta = -1$: note the large number of spurious cells.

List of Tables

Source	Field	a, b, δ	Saliency	Smoothing
NEXRAD	Reflectivity	$20, 60, 1(dBZ)$	$100, 200km^2$	Gaussian ($\sigma = 3km$)
CASA	Reflectivity	$20, 60, 5(dBZ)$	$2.5km^2$	65^{th} percentile within $0.25km$
GOES-12	Infrared	$240, 200, -1(K)$	$160, 500km^2$	None
SEVIRI	Infrared	$235, 144, -20(K)$	$160km^2$	Gaussian ($\sigma = 5km$)

TABLE 1. Parameter values used for the different data sets. The a, b, δ reflect the physical characteristics of the field being processed. For example, the δs for the infrared data sets are negative to enable the algorithm to search for cold tops (lower temperatures). A large δ value can be used to address noise in images with poor spatial resolution, as seen in the SEVIRI parameters. The saliency threshold reflects the spatial resolution of the data. Thus, it can be extremely small for CASA but needs to be quite high for GOES. The smoothing parameters reflect the noisiness of the data. Thus, the noisy CASA dataset was subjected to aggressive smoothing using a rank filter while the clean GOES dataset was not smoothed at all.